Journal of Applied Physics

RESEARCH ARTICLE | SEPTEMBER 17 2024

Low-temperature formation of Ti_2AlN during post-deposition annealing of reactive multilayer systems

Moses O. Nnaji ; David A. Tavakoli ; Dale A. Hitchcock ; Eric M. Vogel

Check for updates

J. Appl. Phys. 136, 115302 (2024)
https://doi.org/10.1063/5.0230405

View Online
Export Citation

13 October 2025 18:15:19

Nanotechnology & Materials Science
Optics & Photonics
Impedance Analysis
Scanning Probe Microscopy
Sensors
Failure Analysis & Semiconductors

Unlock the Full Spectrum.
From DC to 8.5 GHz.
Your Application. Measured.
Find out more
Zurich Instruments

AIP Publishing

Journal of Applied Physics ARTICLE pubs.aip.org/aip/jap

Low-temperature formation of Ti_2AlN during post-deposition annealing of reactive multilayer systems

Cite as: J. Appl. Phys. **136**, 115302 (2024); doi: 10.1063/5.0230405
Submitted: 23 July 2024 · Accepted: 31 August 2024 ·
Published Online: 17 September 2024

View Online Export Citation CrossMark

Moses O. Nnaji,[1] David A. Tavakoli,[1] Dale A. Hitchcock,[2] and Eric M. Vogel[1,a)]

AFFILIATIONS

[1]School of Materials Science and Engineering, Georgia Institute of Technology, Atlanta, Georgia 30332, USA
[2]Savannah River National Laboratory, Savannah River Site, Aiken, South Carolina 29808, USA

[a)]**Author to whom correspondence should be addressed:** eric.vogel@mse.gatech.edu

ABSTRACT

$M_{n+1}AX_n$-phase Ti_2AlN thin-films were synthesized using reactive sputtering-based methods involving the deposition of single-layer TiAlN, and Ti/AlN and TiN/TiAl multilayers of various modulation periods at ambient temperature and subsequent annealing at elevated temperatures. *Ex situ* and *in situ* x-ray diffraction measurements were used to characterize the Ti_2AlN formation temperature and phase fraction. During annealing, Ti/AlN multilayers yielded Ti_2AlN at a significantly lower *in situ* temperature of 650 °C compared to TiN/TiAl multilayers or single-layer TiAlN (750 °C). The results suggest a reactive multilayer mechanism whereby distinct Ti and AlN layers react readily to release exothermic energy resulting in lower phase transition temperatures compared to TiN and TiAl layers or mixed TiAlN. With a modulation period of 5 nm, however, Ti/AlN multilayers yielded Ti_2AlN at a higher temperature of 750 °C, indicating a disruption of the reactive multilayer mechanism due to a higher fraction of low-enthalpy interfacial TiAlN within the film.

© 2024 Author(s). All article content, except where otherwise noted, is licensed under a Creative Commons Attribution (CC BY) license (https://creativecommons.org/licenses/by/4.0/). https://doi.org/10.1063/5.0230405

13 October 2025 18:15:19

I. INTRODUCTION

The $M_{n+1}AX_n$ phases are a class of layered nanolaminate ceramics where M represents a transition metal, A represents a group 12–16 element, and X represents either carbon or nitrogen.[1] These $M_{n+1}AX_n$ phases, or "MAX-phases," often boast a novel combination of metal and ceramic properties. For instance, many MAX-phases are thermally and electrically conductive, easily machinable, resistant to thermal shock, and are known to maintain many of their properties at elevated temperatures due to the thermal stability of their distinct crystal structure.[2–5] Consequently, MAX-phase coatings have attracted interest for potential use in protective coatings,[6–9] Ohmic contacts,[10–13] high-temperature structural applications,[8,14–16] and low friction systems.[17–20] However, only a few MAX-phases have been adopted in industrial applications.[4] In particular, the high temperatures (>600 °C) typically needed to form their complex crystal structures have served as a persistent bottleneck for the widespread adoption of MAX-phase coatings on temperature-sensitive substrates. Reducing the substrate temperature needed to form MAX-phase thin-films is necessary to improve their viability in demanding applications and, thus, improve the performance of said applications.

Reactive multilayers are thin-film systems which exploit exothermic reactions as a form of "stored energy."[21] In this context, layers of distinct reactant materials are deposited at low substrate temperatures where reactions are not spontaneous. Upon increasing the substrate temperature, these exothermic reactions between the reactants become favorable (based on the Gibbs free energies) and further increase the temperature of the film. Thus, the thermal energy associated with the exothermic reactions effectively results in phase transition at a lower substrate temperature, depending on enthalpy. As MAX-phases possess large and complex unit cells, they require significant energy to outcompete binary phases with smaller unit cells[3,5,22]—tailoring the reactive multilayer deposition approach for films with high reactivity and energy may be helpful in forming MAX-phases at desirably low substrate temperatures.

Magnetron sputtering has been validated as a technique for MAX-phase thin-film growth for some time,[23,24] and MAX-phase

© Author(s) 2024

synthesis via post-deposition annealing of sequentially sputtered multilayers has also been reported in the literature.[25–27] Furthermore, the impact of "stored energy" in these systems has been considered previously.[28] However, work explicitly addressing the impact of the reactive multilayer mechanism and multilayer phase composition on MAX-phase nucleation temperature is limited. Thus, comparing the behavior of composite multilayer films with different reactivities (e.g., containing constituent materials with different free energies and enthalpy) may provide insight for reducing the annealing temperature during MAX-phase synthesis. In this work, the evolution of MAX-phase Ti_2AlN in various TiAlN films as a function of annealing temperature is investigated via extensive *in situ* XRD characterization and is explicitly compared for TiAlN films having distinct phase compositions and multilayer structures. In particular, the Ti_2AlN formation temperature is evaluated for multilayer films with Ti/AlN and TiN/TiAl compositions, varying bilayer thicknesses (or "modulation periods") of 5, 14, 33, and 45 nm, as well as between films of single-layer and multilayer morphology.

II. EXPERIMENTAL

A. Thin-film deposition and annealing

TiAlN films having homogeneous, multilayer Ti/AlN, and multilayer TiN/TiAl structures were deposited via magnetron sputtering at ambient temperature and a pressure of 1 mTorr, using Ar (40 SCCM) as the working gas and elemental Ti and Al targets for film deposition. Si wafers with thermally grown SiO_2 layers of >100 nm thickness were used as substrates. A 10 nm thick Ti layer was sputtered on the substrates prior to film deposition to improve adhesion.

The process parameters for the selected films are shown in Table I. For each film, the Ti and Al targets were continuously run at the same power throughout the deposition process. Each target used either RF or DC-power mode, depending on the film. The multilayer films were obtained via sequential deposition by alternatively shuttering either of the Ti and Al targets. For Ti layers, only the Ti target was left open. For TiN and AlN layers, the respective Ti and Al targets were left open with a concurrent flow of N_2 to induce reactive sputtering. After deposition of TiN and AlN layers, both targets were shuttered for an additional 30 s to better allow the sputtering chamber to remove residual N_2 gas and mitigate unwanted nitriding of the metallic layers. For TiAl layers, the Ti target and Al target were opened concurrently. Single-layer TiAlN was obtained by concurrent sputtering of Ti and Al under a flow of N_2. Examples of the multilayer sputtering process and consequent thin-film structures are illustrated in Fig. 1. Following deposition, all films were removed from the sputtering system and subsequently annealed to at least 550 °C. Some films were annealed concurrently with x-ray diffractometry (XRD) measurements ("*in situ* annealing") under N_2 at ambient pressure, while others were annealed in a furnace ("*ex situ* annealing") under vacuum at a pressure of 10^{-6} Torr.

TABLE I. Deposition parameters for as-deposited TiAlN thin-films.

Film	Ti target power (W)	Al target power (W)	N_2 (SCCM)
Ti/AlN, λ = 5 nm	600—RF	600—DC	10
Ti/AlN, λ = 14 nm	600—RF	600—DC	10
Ti/AlN, λ = 45 nm	400—DC	400—RF	15
TiN/TiAl, λ = 5 nm	400—DC	325—RF	10
TiN/TiAl, λ = 14 nm	600—RF	500—DC	10
TiN/TiAl, λ = 33 nm	400—DC	325—RF	10
TiAlN	150—DC	125—RF	2

B. Thin-film characterization

The sputtering process for each film was calibrated so that all films were of comparable elemental composition and the film thickness. To determine the stoichiometry of the films, x-ray photoelectron spectroscopy (XPS) measurements were performed using a Thermo-Scientific spectrometer system using a monochromatic Al K-Alpha x-ray source with an energy of 1486.6 eV, a spot size of 400 μm, and an x-ray gun operating at 15 W. Depth profiles were obtained by etching of the films with an Ar^+ gun running at 3000 eV. Prior to depth profiling, the films were rinsed with acetone, methanol, and propanol. An electron flood gun was utilized to mitigate charging and shifts in binding energy, and metallic Ti 2p at 454.1 eV was used as a binding energy reference. The Ti–Al–N ratio in the films varied somewhat, but were generally similar to the nominal 2:1:1 Ti:Al:N in Ti_2AlN, ranging from 37.5% to 48.4% Ti, 23.6% to 33.0% Al, and 24.6% to 36.2% N. The film thicknesses were estimated via profilometry and ranged from 165 to 250 nm. The stoichiometry and thickness for each film are summarized in Table II. Raman spectroscopy was also utilized to illustrate the formation of Ti_2AlN after the annealing of multilayer Ti/AlN using a Renishaw Qontor Dispersive Raman Spectrometer at a wavelength of 488 nm.

Both *ex situ* and *in situ* XRD measurements were performed to determine the phase composition and crystallographic orientation of the TiAlN films. *Ex situ* glancing-angle XRD θ–2θ measurements were performed in a Panalytical Empyrean diffractometer using Cu Kα radiation at a tube current of 40 mA with the x-ray generator running at 45 kV over a selected 2θ range of 10°–80°. The step interval was 0.013° with a counting time of 198 s for each step, and the incident angle was set at 7°. *In situ* XRD θ–2θ measurements were performed in a Rigaku Smartlab XE XRD diffractometer using Cu Kα radiation at a tube current of 50 mA with the x-ray generator running at 40 kV over the selected 2θ range of 10°–80° (50°–80° not shown). The step interval was 0.04°, with a counting time of 20 s for each step. Scans were performed at a rate of 10° per minute. The diffractograms were obtained in the temperature range of 25–750 °C in N_2 at ambient pressure. The holding time prior to each diffractogram was 20 min.

III. RESULTS AND DISCUSSION

A. Preliminary Ti_2AlN thin-film synthesis and characterization

First, as a preliminary study to recreate the multilayer approach for MAX-phase synthesis, multilayer Ti/AlN (modulation

13 October 2025 18:15:19

© Author(s) 2024

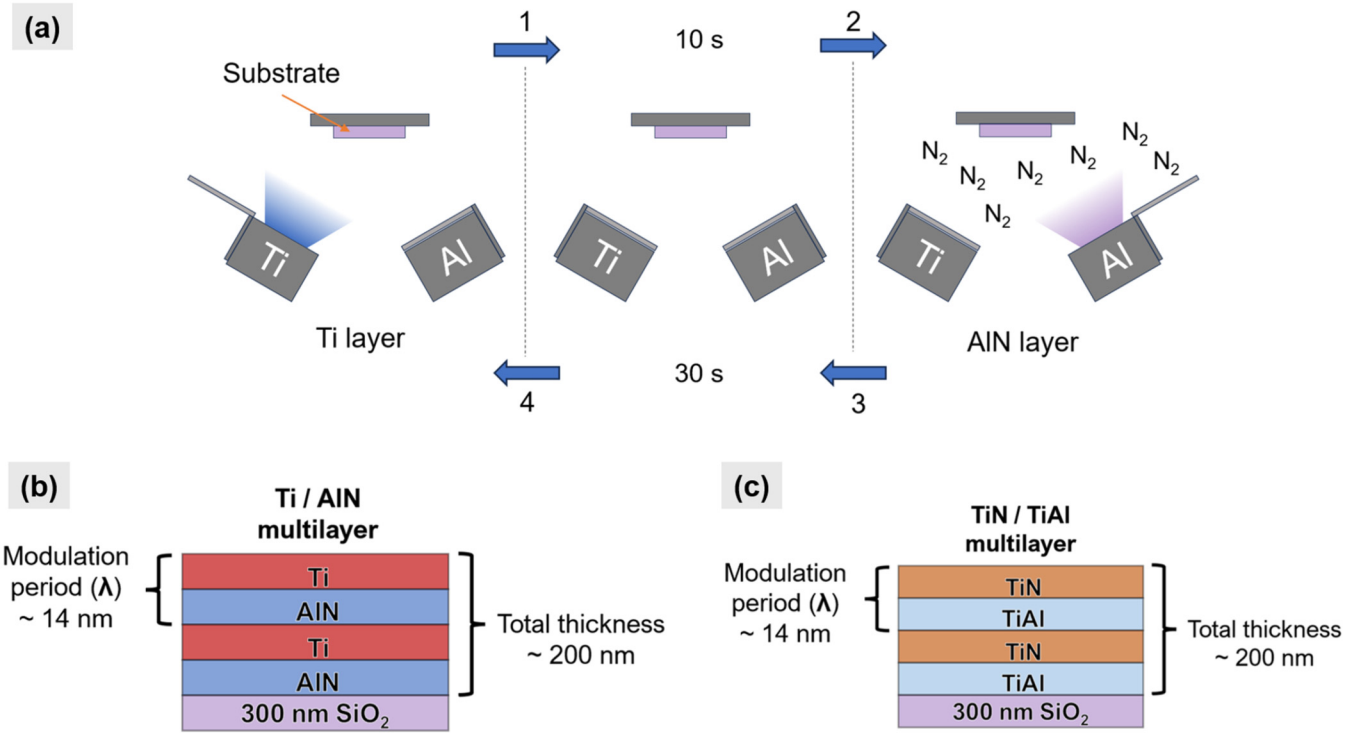

FIG. 1. (a) Example of a Ti/AlN sputtering process flow. (b) Illustration of a Ti/AlN multilayer. (c) Illustration of a TiN/TiAl multilayer.

period = 14 nm) was studied before and after annealing via *ex situ* XRD, Raman spectroscopy, and XPS, which collectively evidenced the formation of MAX-phase Ti_2AlN. XRD scans [Fig. 2(a)] show that as-deposited Ti/AlN films yielded Ti_2AlN with strong c-axis orientation after *ex situ* annealing at 750 °C for 2 h, clearly indicated by the disappearance of the (002) Ti peak at 2θ = 38.0° and the emergence of an intense (002) Ti_2AlN peak at 2θ = 12.9° (PDF 00-018-0070). The (002) Ti peak seems to be shifted compared to the reference (2θ = 38.42°; PDF 00-044-1294), but this may be a consequence of film strain and/or the presence of interleaved AlN layers, where a small (002) AlN peak (2θ = 36.0°; PDF 00-008-0262) may be convoluted with the (002) Ti peak. Raman spectra [Fig. 2(b)] also indicate the formation of Ti_2AlN, as the peaks at 148.3, 228.3, and 354.1 cm^{-1} correspond to the ω_1, ω_2, ω_3, and ω_4 modes produced by 211 MAX-phase lattice vibrations.[29] Furthermore, XPS depth profiles and corresponding elemental Al2p scans [Figs. 2(a)–2(d)] illustrate changes in the Ti/AlN film structure and chemical bonding after annealing. The Ti/AlN film with distinct Ti and AlN layers [Fig. 3(a)] converts into a Ti_2AlN film [Fig. 3(b)] with uniform bulk composition and Al_2O_3 (likely a remnant of a heavily oxidized AlN layer) near the surface. Figure 3(c) shows covalent Al–N bonding within an AlN layer at 74.3 eV, where the small peak at 72.5 eV indicates metallic Al–Ti bonding at Ti–AlN interfaces. Conversely, Fig. 3(d) shows almost entirely metallic Al–Al bonding at 72.5 eV (corresponding to metallic Al monolayers in Ti_2AlN), with Al–O bonding observed at 75.4 eV due to oxidation during the annealing process.

TABLE II. Measured elemental composition and thickness of as-deposited TiAlN thin-films.

Film	Ti (%)	Al (%)	N (%)	Thickness (nm)
Ti/AlN, λ = 5 nm	42.3	24.5	33.2	215
Ti/AlN, λ = 14 nm	37.7	33.2	29.1	200
Ti/AlN, λ = 45 nm	45.0	29.0	26.0	220
TiN/TiAl, λ = 5 nm	45.7	22.5	33.2	250
TiN/TiAl, λ = 14 nm	43.1	29.6	27.3	200
TiN/TiAl, λ = 33 nm	48.4	27.0	24.6	165
TiAlN	40.3	23.6	36.2	200

B. Ti_2AlN growth during *in situ* XRD of TiAlN multilayers

In situ XRD shows that Ti_2AlN forms at 650 °C in multilayer Ti/AlN films [Fig. 4(a)], while it forms at 750 °C in multilayer TiN/TiAl films [Fig. 4(b)]. Unlike in Fig. 2(a), (006) Ti_2AlN peaks are now observed, having been previously undetected due to the fixed x-ray source during glancing-angle XRD.[30] For the TiN/TiAl film,

13 October 2025 18:15:19

© Author(s) 2024

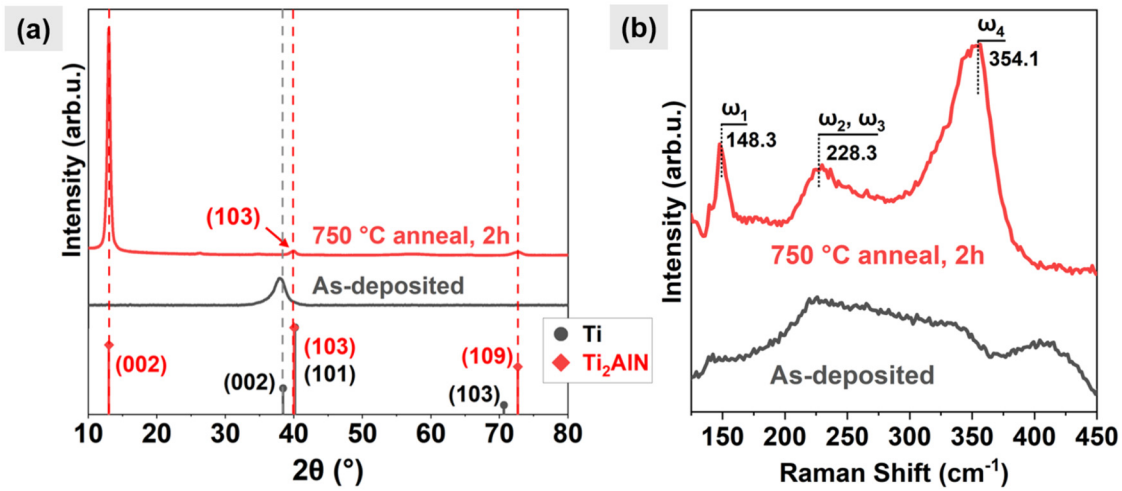

FIG. 2. (a) Glancing-angle XRD of as-deposited and annealed multi-layer Ti/AlN. PDF stick diagrams of Ti and Ti_2AlN are included for reference. (b) Raman spectra of as-deposited and annealed multi-layer Ti/AlN.

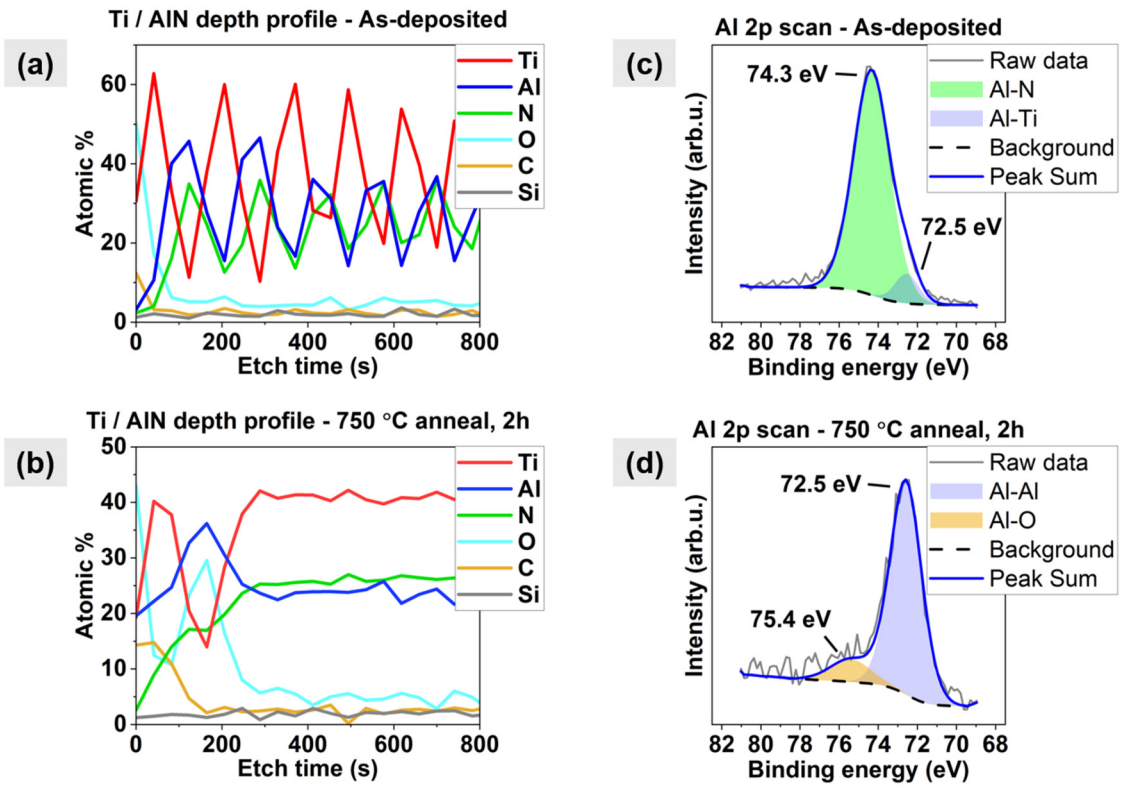

FIG. 3. (a) XPS depth profile of the as-deposited multi-layer Ti/AlN. (b) XPS depth profile of the annealed multi-layer Ti/AlN. (c) Al2p scan taken of an AlN layer within the as-deposited multi-layer Ti/AlN. (d) XPS Al2p scan taken within the bulk of the annealed Ti/AlN (etch time >300 s).

13 October 2025 18:15:19

© Author(s) 2024

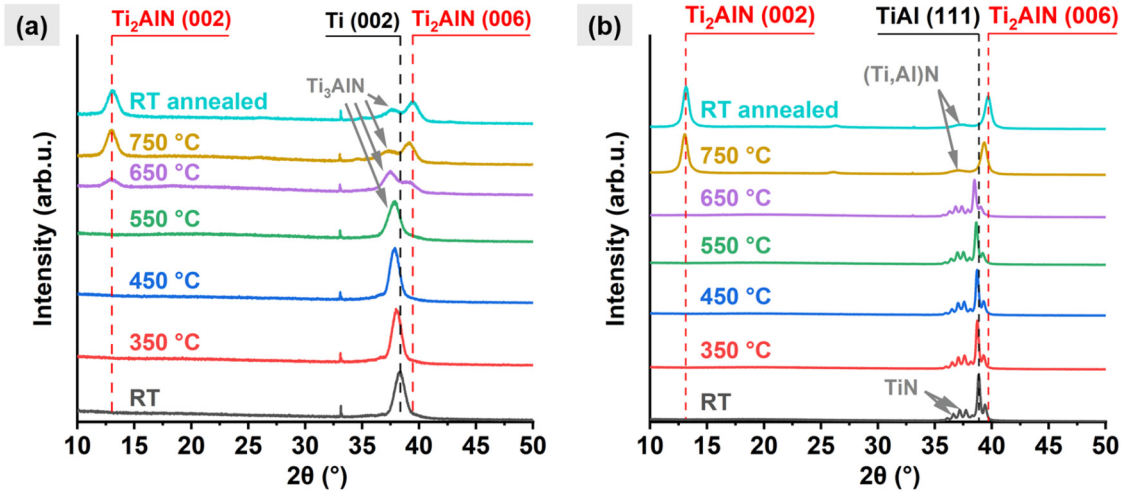

FIG. 4. (a) *In situ* XRD of multilayer Ti/AlN with a modulation period of 14 nm. The peak at 2θ = 33° is from the SiO_2/Si substrate. (b) *In situ* XRD of multilayer TiN/TiAl with a modulation period of 14 nm.

the (111) TiAl peak at 2θ = 38.8° (PDF 00-055-0253) is prominent, while the small peaks around 36.0–37.7° seem to be a peak-splitting artifact caused by thin layers—the center of these peaks is at 2θ = 36.8°, corresponding to (111) TiN (PDF 00-006-0642). The single-layered TiAlN film revealed a weak (111) (Ti,Al)N reflection at 2θ = 37.27° (PDF 04-005-5251), with Ti_2AlN forming at 750 °C [Fig. 5(a)], similarly to the TiN/TiAl film. However, unlike the multilayer films, the Ti_2AlN peak is at 2θ = 40.2° and is distinct from the (006) Ti_2AlN peak at 2θ = 39.4°, instead corresponding to the (103) reflection [Fig. 5(b)]. This indicates a lack of texture,[31] as (103) Ti_2AlN is the most intense of all Ti_2AlN reflections. The intense (002) Ti_2AlN peaks in multilayers could be a consequence of Ti_2AlN adopting the strong c-axis orientation of the as-deposited phases during annealing,[30] although another possibility is the constriction of grain growth direction due to the film structure. In the homogeneous TiAlN, Ti_2AlN grains simply emerge and expand in random locations without preferred orientation. In multilayer films, however, these grains may instead nucleate

13 October 2025 18:15:19

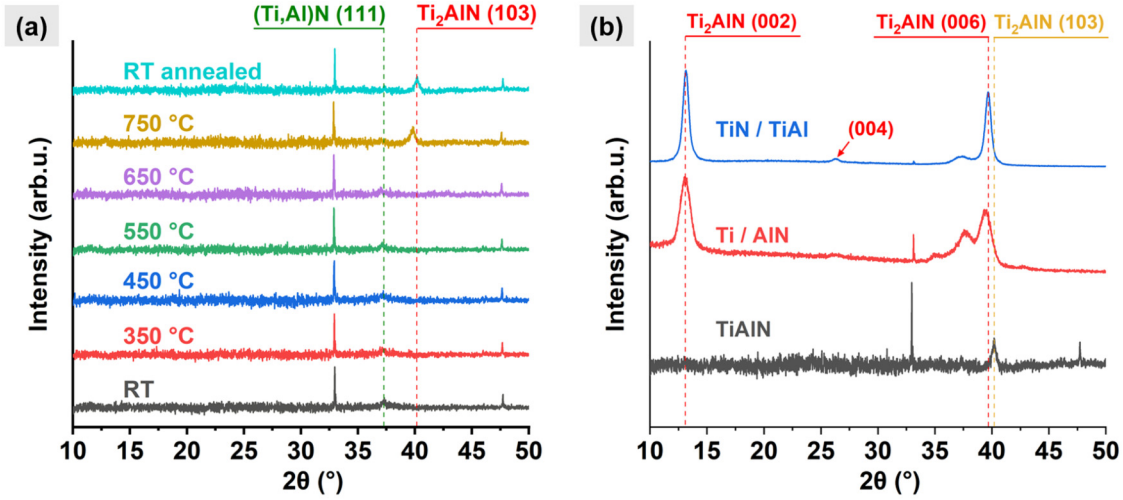

FIG. 5. (a) *In situ* XRD of single-layer TiAlN. The peaks at 2θ = 33° and 2θ = 47.7° are from the substrate. (b) Room temperature XRD scans of TiAlN films after annealing to 750 °C.

© Author(s) 2024

in a lateral fashion at layer interfaces or within specific layers, forming thin Ti_2AlN layers that can only expand along the c-axis as the film is annealed, leading to textured firms—even on amorphous substrates.[26]

Although all films yielded some fraction of MAX-phase Ti_2AlN after annealing, it is apparent that the reaction pathway is affected by the thin-film phase composition. The differences in the as-deposited phase compositions are clearly observed via XRD. *In situ* XRD of the Ti/AlN film indicates the formation of some additional phase that remains to a considerable degree after the annealing process, as evidenced by the ambiguous peak at $2\theta = 37.72°$ [Fig. 4(a)]. This does not align with the initial (002) Ti peak observed at $2\theta = 38.3°$, nor any TiN and TiAl reflections, but instead seems to align more with the (111) peak of the cubic Ti_3AlN phase ($2\theta = 38.87°$; PDF 00-037-1140), where common film effects such as strain may account for the discrepancy in 2θ. Indeed, Ti_3AlN has been proposed as an intermediate phase that forms prior to Ti_2AlN.[31,32] Nonetheless, *in situ* XRD of the TiN/TiAl film does not indicate the formation of any additional phases, unlike Ti/AlN. Instead, the distinct TiN and TiAl layers are preserved until 650–750 °C, whereafter only Ti_2AlN and a trace amount of cubic (111) TiN/(Ti,Al)N are observed [Fig. 4(b)]. These results suggest that the formation of Ti_2AlN in Ti/AlN films begins more gradually at lower temperatures, compared to a more rapid transition at higher temperatures in TiN/TiAl films. Differences in the behavior of Ti/AlN and TiN/TiAl are apparent even when the annealing times are extended: XRD [Fig. 6(a)] indicates the formation of Ti_2AlN in Ti/AlN as early as 550 °C after *ex situ* annealing for 12 h, which is similar to the previously reported minimum synthesis temperatures for Ti-based MAX-phases.[25,32,33] Conversely, Ti_2AlN was not immediately observed in TiN/TiAl following the extended anneal at 550 °C, only appearing in trace amounts after additional *in situ* annealing at 650 °C for 20 min [Fig. 6(b)].

The difference in behavior between Ti/AlN and TiN/TiAl films during annealing might be explained as a consequence of the multilayer reactivity and diffusivity. For instance, Ti is notably reactive, and a proposed mechanism for the formation of an intermediate Ti_3AlN phase is the breakdown and dissolution of the AlN layers into the Ti layers at above 400 °C.[32] It has also been argued that this intermediate phase is instead a single-phase TiAlN solid solution in the form of a distorted hexagonal α-Ti lattice.[25] Closer inspection of the Ti/AlN *in situ* XRD scans provides more insight into the interactions between the Ti and AlN layers and subsequent phase transitions [Figs. 7(a) and 7(b)]. As the annealing temperature increases, the (002) Ti peak shifts to lower 2θ as a consequence of thermal expansion and an increased lattice parameter. This trend continues with increasing temperature (in a non-linear fashion) but encounters a discrepancy around 450–550 °C [Fig. 7(a)]. The FWHM of (002) Ti also changes with temperature, perhaps decreasing slightly as a consequence of enhanced crystallinity during annealing, but increases sharply at 550 °C—the peak widens as the reflection from a different phase separates from (002) Ti [Fig. 7(b)]. Next, Fig. 8 suggests an interesting possibility: the emergence of (111) Ti_3AlN occurs along with the formation of a transient solid solution. As purported by Cabioch *et al.*,[25] once AlN decomposes, Al and N diffuse into Ti to form an α-Ti solid solution, shrinking the Ti lattice and offsetting the effect of thermal expansion—this is apparent as the (002) Ti peak position is static from 450 to 550 °C ($2\theta = 37.85°$). In fact, this transformation might even be indicated at 350–450 °C, where the FWHM of (002) Ti increases slightly [Fig. 7(b)]. However, the shoulder clearly observed at 550 °C aligns more with the peak at 650 °C ($2\theta = 37.43°$), which in turn may align with the (111) Ti_3AlN peak observed at $2\theta = 37.72°$ if cooled to room temperature. At 650 °C, the fraction of the solid solution is minimal, while the intensity of (111) Ti_3AlN increases and Ti_2AlN begins to form. As the annealing temperature increases to 750 °C, the fraction of Ti_2AlN appears

13 October 2025 18:15:19

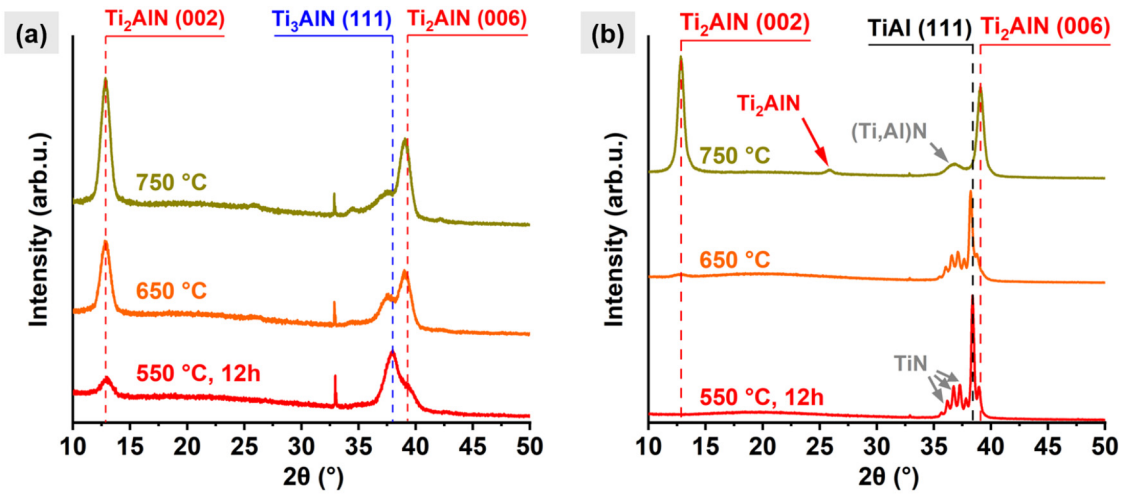

FIG. 6. (a) *In situ* XRD of multilayer Ti/AlN after a 12 h anneal at 550 °C. (b) *In situ* XRD of multilayer TiN/TiAl after a 12 h anneal at 550 °C.

© Author(s) 2024

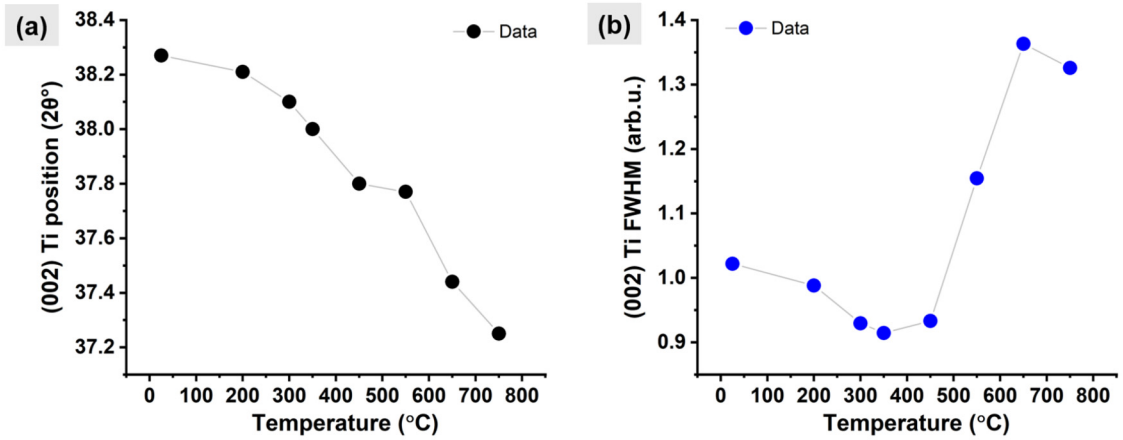

FIG. 7. (a) (002) Ti peak position as a function of annealing temperature. (b) FWHM of the (002) Ti peak as a function of annealing temperature.

to increase at the expense of (111) Ti_3AlN and the (002) Ti peak disappears completely [Fig. 4(a)]. These data suggest that multiple intermediate phases are formed as a consequence of reactions between the Ti and AlN layers at >450 °C. The α-Ti solid solution is unstable and disappears by 650–750 °C, whereas the Ti_3AlN phase is more stable but still yields Ti_2AlN with sufficient annealing temperature and time.

In contrast to Ti, TiN is often reputed as a good diffusion barrier, with high-temperature stability and low Al solubility.[34,35] In the case of TiN/TiAl multilayers, a proposed mechanism for the phase transition to Ti_2AlN is the slow diffusion of N from TiN into TiAl and diffusion of Al from TiAl into TiN[36]—in this case, yielding Ti_2AlN above 650 °C. This Ti_2AlN formation also appears to be more prominent in TiAl layers, as trace amounts of TiN/(Ti, Al)N remain [Figs. 4(b) and 6(b)]. However, it is also possible that the TiN–TiAl reactions are comparably energetic to Ti–AlN reactions but may simply require higher temperatures to actually be favorable. This notion is supported by the thorough phase transitions in TiN/TiAl films observed at 650–750 °C [Fig. 4(b)].

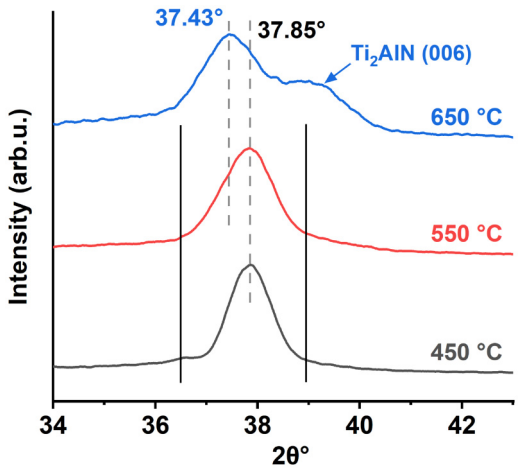

FIG. 8. *In situ* XRD of multilayer Ti/AlN from 450 to 650 °C. Guides are added to help illustrate differences in the position and width of the (002) Ti peak with increasing temperature.

Investigating the effect of the modulation period on Ti_2AlN growth temperature, *in situ* XRD shows that Ti/AlN multilayers with modulation periods of 14 and 45 nm have the same minimum Ti_2AlN formation temperature of 650 °C during *in situ* annealing [Fig. 9(a)]. For the 45 nm period film, the (002) AlN reflection is clearly visible at $2\theta = 36.0°$ due to thicker AlN layers and remains to some degree throughout the annealing process. However, Ti/AlN films with a modulation period of 5 nm did not form Ti_2AlN until 750 °C, despite the presumably shorter diffusion distances [Fig. 9(b)]. XRD for this film also shows an ambiguous peak around $2\theta = 37.5°$, which is closest to (111) Ti_3AlN at 37.87° or (111) (Ti,Al)N at 37.13°, though it is clearly neither from hexagonal Ti or AlN, and is probably from a mixed ternary compound. In this case, the increased formation temperature may be a consequence of the lowered reactivity of the composite film. The Ti–AlN layer interfaces are likely not atomically sharp, having some degree of prematurely mixed Ti–Al–N. As the layers become thinner, these mixed low-energy regions at the layer interfaces comprise a proportionally larger fraction of the film, leading to a lower amount of stored energy compared to films with thicker layers.[21] However, the Ti_2AlN growth temperature in TiN/TiAl films was unaffected by these changes [Figs. 9(c) and 9(d)], where Ti_2AlN formed at 750 °C for modulation periods of 5, 14, and 33 nm. XRD of the 5 nm period TiN/TiAl film is peculiar—the peak at $2\theta = 38.1°$ is quite far from the (111) TiAl reflection at 38.7°, and a peak-splitting artifact is again visible due to the thin layers, where small peaks at $2\theta = 36.3°$ and 39.9° are the same distance away from the peak at 38.1°. Still, this structure behaves like the other TiN/TiAl films in that the phase integrity and distinct layers are

13 October 2025 18:15:19

© Author(s) 2024

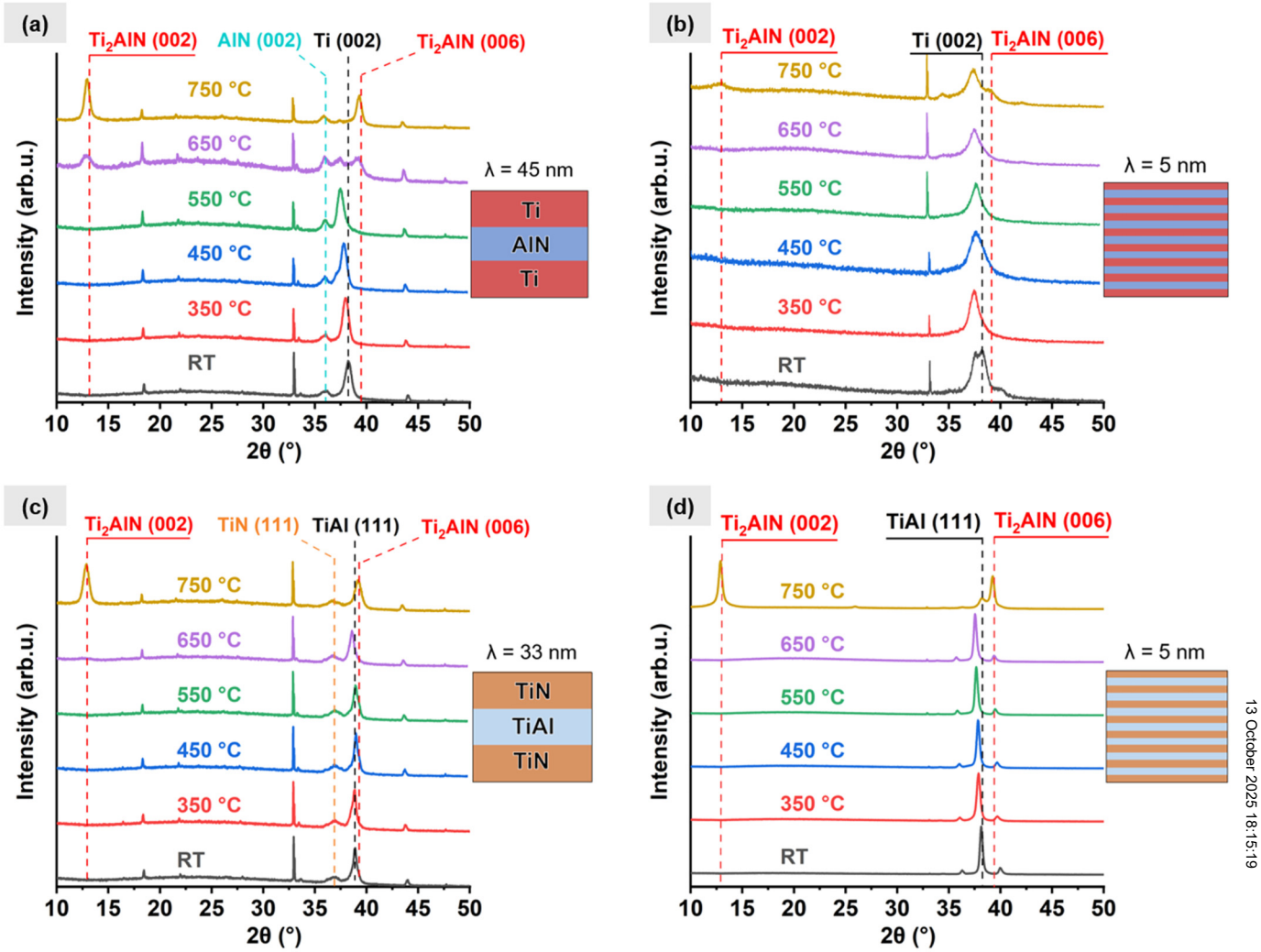

FIG. 9. (a) *In situ* XRD of multilayer Ti/AlN with a period of 45 nm. (b) *In situ* XRD of multilayer Ti/AlN with a period of 5 nm. (c) *In situ* XRD of multilayer TiN/TiAl with a period of 45 nm. (d) *In situ* XRD of multilayer TiN/TiAl with a period of 5 nm.

maintained until 750 °C, whereafter intense (002) Ti_2AlN appears. This might indicate the presence of TiAl layers that, while heavily distorted, maintains their crystal structure.

C. (002) Ti_2AlN area fraction

As a rough estimate of the Ti_2AlN phase fraction after *in situ* annealing, the area fraction (i.e., relative intensity) of the (002) Ti_2AlN peak was evaluated in multilayer films and noted to be affected by changes in the modulation period (Fig. 10). Here, the area fraction is simply defined as the ratio of the (002) Ti_2AlN peak area to the total area of all (002) and (111) peaks detected in a given film—the (002) and (111) peaks are selected as the characteristic reflections for each phase due to the strong c-axis orientation of the multilayer films. For Ti/AlN, the fraction of (002) Ti_2AlN varied significantly based on the modulation period, while the TiN/TiAl films yield a consistently high fraction of (002) Ti_2AlN. Clearly, these variations in layer thicknesses had a more pronounced impact on the Ti/AlN multilayers compared to the TiN/TiAl multilayers. This suggests that the Ti_2AlN growth temperature in Ti/AlN multilayers is indeed influenced by heightened multilayer reactivity, being that Ti_2AlN formation is more strongly disrupted by a higher fraction of low-energy interfacial regions in these films. Conversely, the minimal effect of period variations in TiN/TiAl films may indicate that their multilayer reactivity is less impactful for Ti_2AlN formation, at least below 750 °C. This is reasonable if TiN is regarded as inert compared to Ti at such temperatures.

13 October 2025 18:15:19

© Author(s) 2024

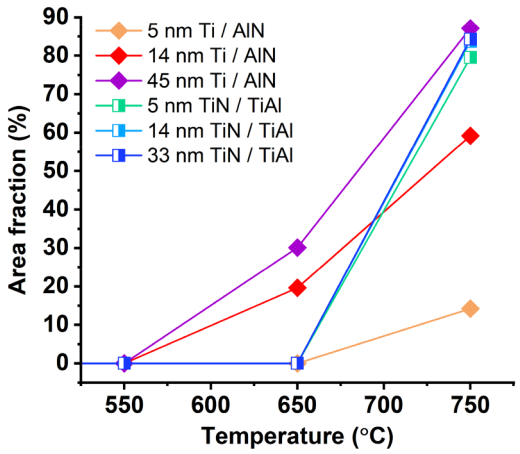

FIG. 10. Area fraction of (002) Ti_2AlN in multilayer films as a function of *in situ* annealing temperature.

IV. SUMMARY AND CONCLUSIONS

In this work, MAX-phase Ti_2AlN was obtained at different annealing temperatures by implementing various sputtering approaches which adjusted the phase compositions and modulation periods of as-deposited composite TiAlN films. The as-deposited phase composition was found to be a crucial factor with regard to Ti_2AlN growth temperature: Ti/AlN multilayers with a modulation period of 14–45 nm yielded the lowest Ti_2AlN growth temperature at 650 °C via *in situ* annealing, compared to 750 °C for single-layer TiAlN and TiN/TiAl. Additionally, following extended *ex situ* annealing at 550 °C for 12 h, Ti/AlN multilayers ($\lambda = 14–45$ nm) formed some Ti_2AlN at 550 °C, while TiN/TiAl multilayers required additional *in situ* annealing up to 650 °C before trace amounts of Ti_2AlN were observed.

Low Ti_2AlN formation temperatures in Ti/AlN are enabled by high film reactivity derived from distinct Ti and AlN layers, which decompose around 450–550 °C. One notion is that Ti/AlN releases stored energy during annealing in larger quantities (higher enthalpy) and/or at lower temperatures (lower Gibbs free energy) than TiN/TiAl. Another factor is the presence of intermediate phases uniquely formed in annealed Ti/AlN—possibly, the crystal structures of the α-Ti solid solution or Ti_3AlN allow Ti_2AlN to emerge at comparatively low temperatures. However, Ti/AlN with a modulation period of 5 nm exhibited diminished multilayer reactivity due to the prominence of mixed low-energy TiAlN at the layer interfaces, forming Ti_2AlN at an increased temperature of 750 °C. For low-temperature synthesis of MAX-phase films in the future, it may be useful to synthesize multilayers with energetic constituent layers having sufficient low-temperature reactivity, in tandem with extensive transmission electron microscopy characterization to develop atomically sharp layer interfaces.

ACKNOWLEDGMENTS

This work was performed in part at the Georgia Tech Institute for Electronics and Nanotechnology, a member of the National Nanotechnology Coordinated Infrastructure, which is supported by the National Science Foundation (NSF) (Grant No. ECCS-1542174). This material is based upon work supported by the U.S. Department of Energy, Office of Science, Fusion Energy Sciences Program Office's Fusion Materials Research Program under Contract No. SCW0138. This work was produced in part by Battelle Savannah River Alliance, LLC under Contract No. 89303321CEM000080 with the U.S. Department of Energy. Publisher acknowledges the U.S. Government license to provide public access under the DOE Public Access Plan (http://energy.gov/downloads/doe-public-access-plan).

AUTHOR DECLARATIONS

Conflict of Interest

The authors have no conflicts to disclose.

Author Contributions

Moses O. Nnaji: Conceptualization (equal); Data curation (equal); Formal analysis (equal); Investigation (equal); Methodology (equal); Visualization (equal); Writing – original draft (equal); Writing – review & editing (equal). **David A. Tavakoli:** Data curation (supporting); Funding acquisition (supporting); Methodology (supporting); Project administration (equal); Resources (equal); Supervision (equal); Writing – review & editing (equal). **Dale A. Hitchcock:** Funding acquisition (equal); Project administration (equal); Resources (equal); Supervision (equal); Writing – review & editing (equal). **Eric M. Vogel:** Data curation (equal); Funding acquisition (equal); Methodology (equal); Project administration (equal); Resources (equal); Supervision (equal); Writing – review & editing (equal).

DATA AVAILABILITY

The data that support the findings of this study are available from the corresponding author upon reasonable request.

REFERENCES

[1]M. W. Barsoum, Prog. Solid State Chem. **28**(1–4), 201–281 (2000).
[2]M. W. Barsoum and T. El-Raghy, J. Am. Ceram. Soc. **79**(7), 1953–1956 (1996).
[3]P. Eklund, M. Beckers, U. Jansson, H. Högberg, and L. Hultman, Thin Solid Films **518**(8), 1851–1878 (2010).
[4]J. Gonzalez-Julian, J. Am. Ceram. Soc. **104**(2), 659–690 (2021).
[5]P. Eklund, J. Rosen, and P. O. Å. Persson, J. Phys. D: Appl. Phys. **50**(11), 113001 (2017).
[6]T. Go, Y. J. Sohn, G. Mauer, R. Vaßen, and J. Gonzalez-Julian, J. Eur. Ceram. Soc. **39**(4), 860–867 (2019).
[7]Z. Wang, G. Ma, L. Liu, L. Wang, P. Ke, Q. Xue, and A. Wang, Corros. Sci. **167**, 108492 (2020).
[8]J. L. Smialek, Metall. Mater. Trans. A **49**(3), 782–792 (2018).
[9]H. Shi, R. Azmi, L. Han, C. Tang, A. Weisenburger, A. Heinzel, J. Maibach, M. Stüber, K. Wang, and G. Müller, Corros. Sci. **201**, 110275 (2022).
[10]M. A. Borysiewicz, E. Kamińska, A. Piotrowska, I. Pasternak, R. Jakieła, and E. Dynowska, Acta Phys. Pol., A **114**(5), 1061–1066 (2008).
[11]H. Fashandi, M. Andersson, J. Eriksson, J. Lu, K. Smedfors, C.-M. Zetterling, A. Lloyd Spetz, and P. Eklund, Scr. Mater. **99**, 53–56 (2015).
[12]B. Pécz, L. Tóth, M. A. Di Forte-Poisson, and J. Vacas, Appl. Surf. Sci. **206**(1–4), 8–11 (2003).

13 October 2025 18:15:19

© Author(s) 2024

[13]T. Abi-Tannous, M. Soueidan, G. Ferro, M. Lazar, B. Toury, M. F. Beaufort, J. F. Barbot, J. Penuelas, and D. Planson, Appl. Surf. Sci. **347**, 186–192 (2015).
[14]J. Gonzalez-Julian, T. Go, D. E. Mack, and R. Vaßen, Surf. Coat. Technol. **340**, 17–24 (2018).
[15]N. P. Padture, M. Gell, and E. H. Jordan, Science **296**(5566), 280–284 (2002).
[16]J. L. Smialek, B. J. Harder, and A. Garg, Surf. Coat. Technol. **285**, 77–86 (2016).
[17]S. Myhra, J. W. B. Summers, and E. H. Kisi, Mater. Lett. **39**(1), 6–11 (1999).
[18]T. El-Raghy, P. Blau, and M. W. Barsoum, Wear **238**(2), 125–130 (2000).
[19]J. Gonzalez-Julian, J. Llorente, M. Bram, M. Belmonte, and O. Guillon, J. Eur. Ceram. Soc. **37**(2), 467–475 (2017).
[20]Y. Zhang, Z. Sun, and Y. Zhou, Mater. Res. Innovations **3**(2), 80–84 (1999).
[21]D. P. Adams, Thin Solid Films **576**, 98–128 (2015).
[22]V. Vishnyakov, J. Lu, P. Eklund, L. Hultman, and J. Colligon, Vacuum **93**, 56–59 (2013).
[23]J.-P. Palmquist, U. Jansson, T. Seppänen, P. O. Å. Persson, J. Birch, L. Hultman, and P. Isberg, Appl. Phys. Lett. **81**(5), 835–837 (2002).
[24]T. Joelsson, A. Hörling, J. Birch, and L. Hultman, Appl. Phys. Lett. **86**(11), 111913 (2005).
[25]T. Cabioch, M. Alkazaz, M.-F. Beaufort, J. Nicolai, D. Eyidi, and P. Eklund, Mater. Res. Bull. **80**, 58–63 (2016).
[26]L. Gröner, L. Kirste, S. Oeser, A. Fromm, M. Wirth, F. Meyer, F. Burmeister, and C. Eberl, Surf. Coat. Technol. **343**, 166–171 (2018).
[27]D. L. Ma, Q. Y. Deng, H. Y. Liu, Y. T. Li, and Y. X. Leng, Surf. Coat. Technol. **425**, 127749 (2021).
[28]C. Tang, M. Steinbrück, M. Klimenkov, U. Jäntsch, H. J. Seifert, S. Ulrich, and M. Stüber, J. Vac. Sci. Technol. A **38**(1), 013401 (2020).
[29]V. Presser, M. Naguib, L. Chaput, A. Togo, G. Hug, and M. W. Barsoum, J. Raman Spectrosc. **43**(1), 168–172 (2012).
[30]R. Grieseler, T. Kups, M. Wilke, M. Hopfeld, and P. Schaaf, Mater. Lett. **82**, 74–77 (2012).
[31]Y. Yang, M. Keunecke, C. Stein, L.-J. Gao, J. Gong, X. Jiang, K. Bewilogua, and C. Sun, Surf. Coat. Technol. **206**(10), 2661–2666 (2012).
[32]C. Höglund, M. Beckers, N. Schell, J. V. Borany, J. Birch, and L. Hultman, Appl. Phys. Lett. **90**(17), 174106 (2007).
[33]Z. Wang, W. Li, Y. Liu, J. Shuai, P. Ke, and A. Wang, Appl. Surf. Sci. **502**, 144130 (2020).
[34]J. C. Schuster and J. Bauer, J. Solid State Chem. **53**(2), 260–265 (1984).
[35]Q. Chen and B. Sundman, J. Phase Equilib. **19**(2), 146–160 (1998).
[36]V. Dolique, M. Jaouen, T. Cabioc'h, F. Pailloux, P. Guérin, and V. Pélosin, J. Appl. Phys. **103**(8), 083527 (2008).

13 October 2025 18:15:19

© Author(s) 2024